Hydrophilic or Hydrophobic? Optimizing the Catalyst Microenvironment for Gas-Involving Electrocatalysis

Kaige Shi,[1] Zhuanghe Ren,[1] Zhen Meng,[2] and Xiaofeng Feng[1,2,3,4]*

[1]Department of Physics, University of Central Florida, Orlando, Florida 32816, United States

[2]Department of Chemistry, University of Central Florida, Orlando, Florida 32816, United States

[3]Renewable Energy and Chemical Transformations (REACT) Cluster, University of Central Florida, Orlando, Florida 32816, United States

[4]Department of Materials Science and Engineering, University of Central Florida, Orlando, Florida 32816, United States

*Email: Xiaofeng.Feng@ucf.edu (X.F.)

Abstract:

Electrocatalysis plays a key role in the development of renewable energy technologies. Along with the design of electrocatalysts, the microenvironment around catalytic sites has received increasing attention because it affects the distribution and mass transport of reaction species and impacts the reaction kinetics. In this Concept article, we highlight some mechanistic insights into the effect of microenvironment on gas-involving electrocatalytic reactions, including CO_2 reduction, 2-electron oxygen reduction, and hydrazine oxidation, demonstrating their sensitivity to the wetting properties of microenvironment. For reactions with a gaseous reactant, a moderately hydrophobic microenvironment can greatly enhance the mass transport of gaseous species to accelerate the reaction kinetics while improving the stability of gas-diffusion electrodes. In contrast, for reactions with a liquid reactant and gaseous product, a hydrophilic microenvironment improves the exposure of catalytic sites to the reactant, while a hydrophobic microenvironment benefits the reaction on the other end by accelerating the diffusion and detachment of generated gas bubbles, which would otherwise block the catalytic sites from the reactant. These understandings and insights can provide important guidelines on the control and optimization of microenvironment for the development of efficient electrolyzers.

1. Introduction

Electrocatalysis enables a promising route for the sustainable synthesis of chemicals and fuels using renewable electricity, which can reduce the fossil fuel consumption and carbon emissions to mitigate the impact of human activities on the Earth's ecosystem.[1,2] For example, electrochemical CO_2 reduction reaction (CO_2RR) can convert CO_2 to CO, formate, as well as C_{2+} hydrocarbons and oxygenates.[3–5] Nitrogen reduction reaction (NRR) can enable the electrosynthesis of ammonia, a key ingredient in agricultural fertilizers, so it may provide a sustainable alternative to the energy- and carbon-intensive Haber-Bosch process.[6–8] The 2-electron oxygen reduction reaction (ORR) can enable the electrosynthesis of H_2O_2 from O_2,[9–12] and the hydrogen evolution reaction (HER) produces hydrogen as a clean carbon-free energy carrier. Among the numerous studies of electrocatalysis, most efforts have focused on the design of catalytic materials, understanding the structure-activity relationships, and improving their performance metrics.[13,14] Along with these studies, the catalyst microenvironment, ranging from a few nanometers to a few micrometers away from the catalytic sites, has been found to play an important role in determining the electrocatalytic performance.[15] For example, the local concentration of reaction species and the pH and cations in the local electrolyte were found to have a strong impact on the activity and selectivity of many electrocatalytic reactions.[16–19]

Those important electrocatalytic reactions often involve gaseous species, as either reactants or products, so a balance must be reached between three phases: solid catalyst, liquid electrolyte, and gaseous reactant or product, as schematically illustrated in Figure 1.[20,21] For gas-consuming reactions, the presence of gas-phase reactant near catalytic sites can accelerate the mass transport of the reactant.[20] For gas-evolving reactions, it is essential to remove the generated gas bubbles from the catalyst surface in a timely manner so that the active sites can be exposed to liquid reactant again.[21] Therefore, an important property of the microenvironment is the wetting characteristic, as a hydrophilic surface (contact angle < 90°) favors liquid while a hydrophobic surface (contact angle > 90°) favors gas.[22] The wetting properties can affect the distribution and diffusion of liquid and gaseous species around catalytic sites, and thus impact the reaction kinetics.[23–26] Accordingly, many efforts have been made to improve gas-involving electrocatalysis by designing electrodes with optimized wetting properties. For example, one strategy is to prepare electrodes with nanostructured morphology such as nanowires or nanotubes with tunable wetting properties.[27–29] However, the most widely used electrocatalyst formulation is dispersion of metal nanoparticles on carbon black to form a porous electrode, where the wetting characteristic of the carbon support dominates the catalyst microenvironment, but its significance has been largely overlooked.

In this article, we highlight some mechanistic insights into the effect of microenvironment on gas-involving electrocatalysis, with a focus on the wetting properties. Particularly, we discuss gas-

consuming reactions such as CO_2RR and $2e^-$ ORR, as well as gas-evolving reaction such as N_2H_4 electro-oxidation. We first demonstrate the effect of a hydrophobic microenvironment on CO_2RR by adding polytetrafluoroethylene (PTFE) nanoparticles in the catalyst layer to tune the wetting properties, which can enhance the CO_2RR activity and C_{2+} selectivity. For the electrosynthesis of H_2O_2 on heteroatom-doped carbon black, the doping creates new active sites but also changes the wetting properties of the microenvironment, exhibiting an interplay between the active sites and microenvironment in determining the reaction kinetics. Furthermore, the doped carbon black can be used as catalyst support with tunable wetting properties for gas-evolving reactions such as N_2H_4 electro-oxidation, where the microenvironment governs the exposure of active sites to the reactant and the removal of generated gas bubbles. Our research provides new understandings on the effect of microenvironment in gas-involving electrocatalysis for the design of efficient electrolyzers.

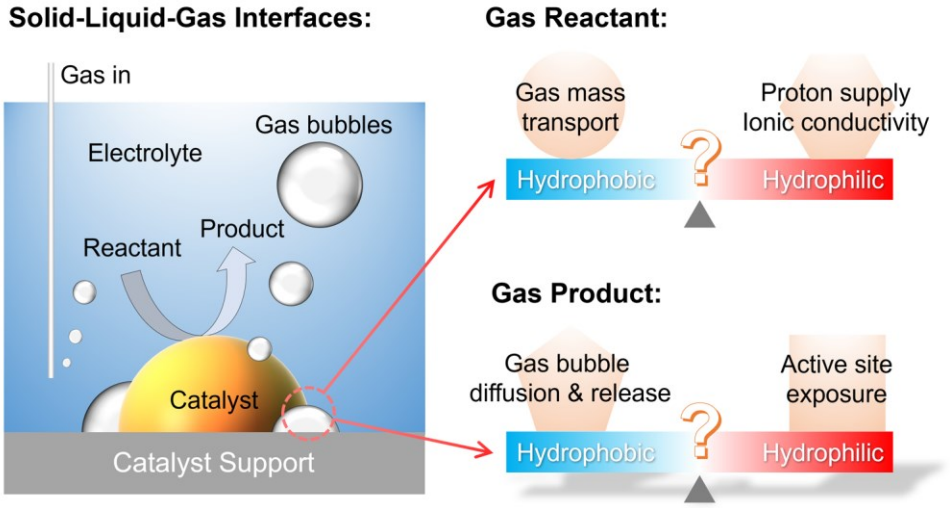

Figure 1. Schematic illustration of the catalyst microenvironment in electrocatalytic reactions with gaseous reactant or product, with the influence of different factors exhibited on the right side.

2. Effect of a hydrophobic microenvironment on CO_2 electrolysis

We start with the CO_2RR as a representative electrocatalytic reaction with gaseous reactant. A major challenge in developing efficient CO_2 electrolyzers lies in the low solubility and slow diffusion of the reactant in aqueous electrolyte. CO_2 has a solubility of ~33 mM in water, which results in a limiting current density of the order of 10 mA cm^{-2} in conventional H-cell, where CO_2 dissolves in the electrolyte and then diffuses through a thick layer of electrolyte (>100 μm) to reach the catalyst surface where the reaction occurs.[30] To overcome the mass transport limitation, gas-diffusion electrodes (GDEs) have been developed and utilized, where gas-phase reactant diffuses through a microporous layer (MPL) to reach the catalyst layer that is in contact with electrolyte,[31]

as illustrated in Figure 2a. Compared to the slow diffusion through the bulk electrolyte in H-cell, the GDE configuration greatly reduces the diffusion layer thickness of CO_2 and enables current densities >200 mA cm^{-2} for CO_2 electrolysis.[31] Nevertheless, the pores in the catalyst layer are typically filled by liquid electrolyte, so that gas reactant needs to diffuse through the catalyst layer in aqueous phase, which still imposes a limitation on the mass transport of CO_2. Moreover, due to the lack of persistent hydrophobicity,[32] the pores in the GDE generally becomes flooded by the electrolyte after operation for some time, which blocks the gas-diffusion channels in the GDE and suppresses the mass transport of CO_2.

To overcome this challenge, we created a hydrophobic microenvironment in the GDE for CO_2 electrolysis by uniformly dispersing PTFE nanoparticles in the catalyst layer, as illustrated in Figure 2a. The hydrophobic PTFE particles can repel liquid electrolyte and trap gaseous species near the catalyst, thus reducing the CO_2 diffusion layer thickness and improving the mass transport and reaction kinetics beyond the gas-liquid interface.[26] To examine the effect of the hydrophobic microenvironment, CO_2 electrolysis was evaluated on Cu nanoparticle catalysts with and without PTFE nanoparticles in the catalyst layer, as compared in Figure 2b. The partial current densities for CO_2RR on the Cu/C/PTFE electrode were generally higher than that on the Cu/C electrode in the potential range of −0.5 to −1.0 V vs the reversible hydrogen electrode (RHE), suggesting a significant improvement of the reaction kinetics by the hydrophobic microenvironment created by PTFE. The hydrophobic pores enabled by the added PTFE particles can trap gas-phase CO_2 in the catalyst layer and thus largely reduce the diffusion layer thickness in the catalyst layer to accelerate the mass transport of CO_2.[20,23]

The microenvironment in the catalyst layer depends on the loading of PTFE nanoparticles: the higher the loading, the more hydrophobic the microenvironment. To identify the relatively optimal microenvironment, we investigated the effect of the mass ratio of PTFE in the catalyst layer on the CO_2RR performance. As shown in Figure 2c, the partial current densities for CO_2RR exhibited a volcano-shaped relationship with the PTFE mass ratio, indicating that a moderately hydrophobic microenvironment is most beneficial for the CO_2RR. Interestingly, excessive PTFE loading decreased the CO_2RR activity, as a too hydrophobic microenvironment can suppress the availability of protons and ionic conductivity, as confirmed by the decrease of electrochemically active surface area (ECSA), that is, the electrode area wetted by the electrolyte.[23] The hydrophobic microenvironment not only increased the CO_2RR activity, but also enhanced the selectivity for C_{2+} products such as ethylene and ethanol.[20] As shown in Figure 2d, the total Faradaic efficiency for CO_2RR also increased with the PTFE mass ratio, while it did not decrease like the trend of CO_2RR current density at a higher ratio of 70%. Considering the higher CO_2 concentration near the catalyst benefiting from the faster mass transport of CO_2 molecules, the coverage of adsorbed $*CO_2$ on the catalyst surface should therefore increase and thus enhance the CO_2RR activity. The hydrophobic

pores around PTFE nanoparticles in the catalyst layer may also trap the produced CO to increase its local concentration and thus promote the C-C coupling, explaining the higher selectivity of C_{2+} products (Figure 2d).[33] In addition, the hydrophobic microenvironment could mitigate the stability issue of regular GDEs caused by the flooding of liquid electrolyte, benefiting from the persistent hydrophobicity of the added PTFE nanoparticles.[32]

In addition to our work, some other approaches were also applied to tune the hydrophobicity in the GDE, such as optimizing the PTFE loading in the GDE support,[34] embedding hydrophobic particles,[35] adding hydrophobic coatings,[36,37] and sputtering of Cu catalyst on PTFE membranes,[38] where the increase of GDE hydrophobicity generally improved the activity, C_{2+} selectivity, and stability of CO_2 electrolysis. Furthermore, such a hydrophobic microenvironment may be utilized to improve the mass transport and reaction kinetics of other gas-consuming reactions, such as NRR, which also suffers from a low solubility and slow diffusion of the gaseous reactant.[39]

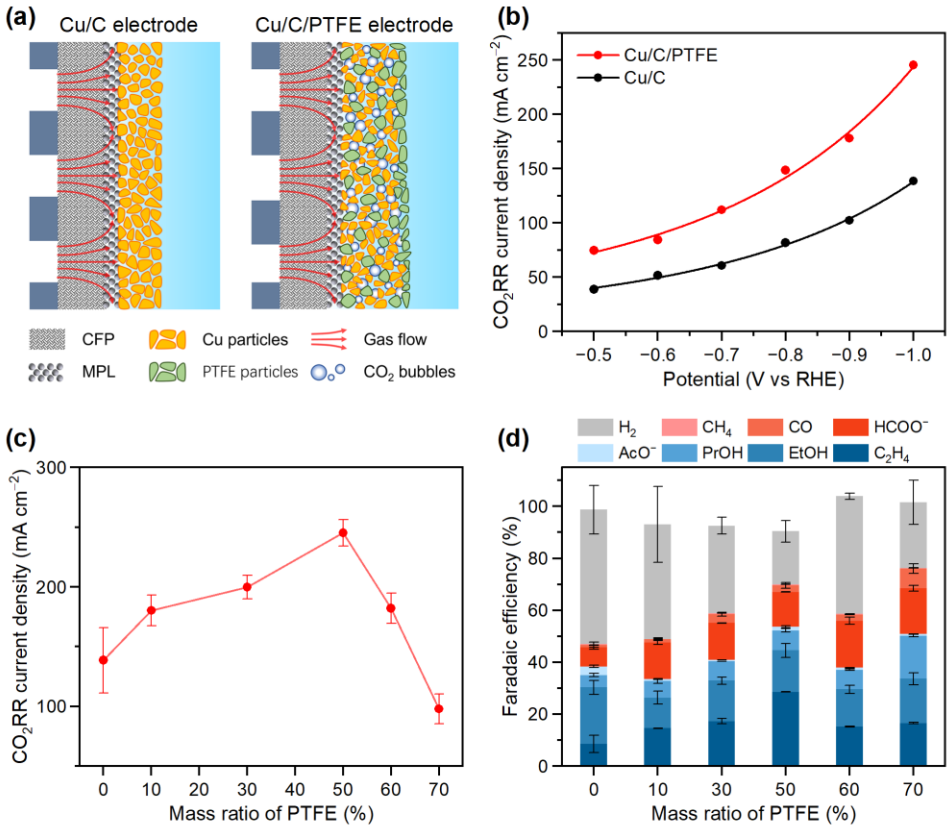

Figure 2. Effect of a hydrophobic microenvironment on CO_2RR in a GDE flow cell. (a) Schematic illustrations of a regular GDE (left) and a GDE with PTFE nanoparticles dispersed in the catalyst layer to create a hydrophobic microenvironment (right). (b) Partial current densities for CO_2RR on the Cu/C and Cu/C/PTFE electrodes in the GDE flow cell at different potentials. (c) Partial current

densities and (d) Faradaic efficiencies for CO_2RR at −1.0 V vs RHE on the Cu/C/PTFE electrodes with different mass ratios of PTFE in the catalyst layer. Adapted with permission from Ref 20.

3. Interplay of active sites and microenvironment in H_2O_2 electrosynthesis

In the above example, a hydrophobic microenvironment was created for CO_2RR by adding PTFE nanoparticles in the catalyst layer, which is "extrinsic" to the Cu electrocatalyst and does not participate in the reaction. However, an excessive loading of PTFE may limit the availability of protons and ionic conductivity and block some catalytic sites. To look further into the effect of microenvironment, we discuss the electrosynthesis of H_2O_2 via $2e^-$ ORR on carbon electrocatalyst. Carbon nanomaterials have been reported as a promising catalyst for the $2e^-$ ORR to produce H_2O_2,[9,10,40–43] but still suffer from low selectivity due to the competitive $4e^-$ process to form H_2O. Introduction of heteroatom dopants such as N, O, B, S, and F can optimize the binding energy of reaction intermediate *OOH to promote the production of H_2O_2.[9,12] However, in parallel with the creation of new active sites, the doping also "intrinsically" changes the wetting properties of the microenvironment around the active sites, which will impose an impact on the mass transport and reaction kinetics.[44] Thus, the active sites and microenvironment may work together to determine the catalytic performance of doped-carbon catalyst for H_2O_2 electrosynthesis.[45]

We adopted the widely used Vulcan XC-72 carbon black and introduced oxygen or fluorine dopants to create new active sites, which simultaneously changed its wetting properties: O-doping increased the hydrophilicity while F-doping made it more hydrophobic.[9,46] Contact angles were measured on the carbon samples with different O- or F-doping levels to analyze the changes of their wetting properties, as exhibited in Figure 3a and 3b, respectively. For the O-doped carbon samples prepared by acidification treatment, the contact angle decreased along with the increase of the acidification time or O-doping level: it decreased from 150° on the pristine carbon black to 108°, 83°, 71°, and 57° on the C-O-3h, C-O-6h, C-O-9h, and C-O-12h electrodes, respectively, indicating an increase of the hydrophilicity by the O-doping. Furthermore, the contact angles were measured on the electrodes after 1-h electrochemical test, as shown in Figure 3a, which all reduced to a certain degree but maintained the same trend with the O-doping level. Interestingly, compared to the pristine carbon black, the contact angles of the as-prepared F-doped carbon samples were just slightly higher, as the carbon black was already very hydrophobic. However, the electrodes often become less hydrophobic after being tested for electrochemical reactions. Therefore, contact angles were further measured on the post-reaction F-doped electrodes, as exhibited in Figure 3b, which dropped to 66°, 82°, 88°, 92°, and 104° for the pristine carbon black, C-F-200, C-F-400, C-F-600, and C-F-800, respectively. Therefore, only the contact angles measured on the post-reaction electrodes can reflect their actual hydrophobicity that can be maintained during electrolysis, which

should be used to compare the wetting properties of the microenvironment. As a result, the post-reaction contact angle increased monotonically with the F-doping level, confirming an increase of hydrophobicity of the microenvironment around catalytic sites by the F-doping.

Rotating ring-disk electrode (RRDE) measurements were performed to evaluate the intrinsic activity of the doped-carbon catalysts, where the mass transport is dominated by convection and can be controlled by the rotation speed (Figure 3c), thus eliminating the influence of reactant mass transport.[47] As shown in Figure 3d and 3e, the partial current densities for H_2O_2 production at 0.6 V vs RHE increased monotonically with the increase of O- or F-doping level in the RRDE measurements, confirming an improvement of the intrinsic activity for H_2O_2 production on both O-doped and F-doped carbon catalysts. The improvement is attributed to the introduction of new active sites for the $2e^-$ ORR to H_2O_2, likely from the oxygen functional groups such as −COOH and C−O−C on O-doped carbon.[9] For the F-doped carbon, the introduced $-CF_2$ functional groups are considered to promote the formation of H_2O_2 due to their moderate binding energy with *OOH, a key reaction intermediate for selective H_2O_2 production.[48]

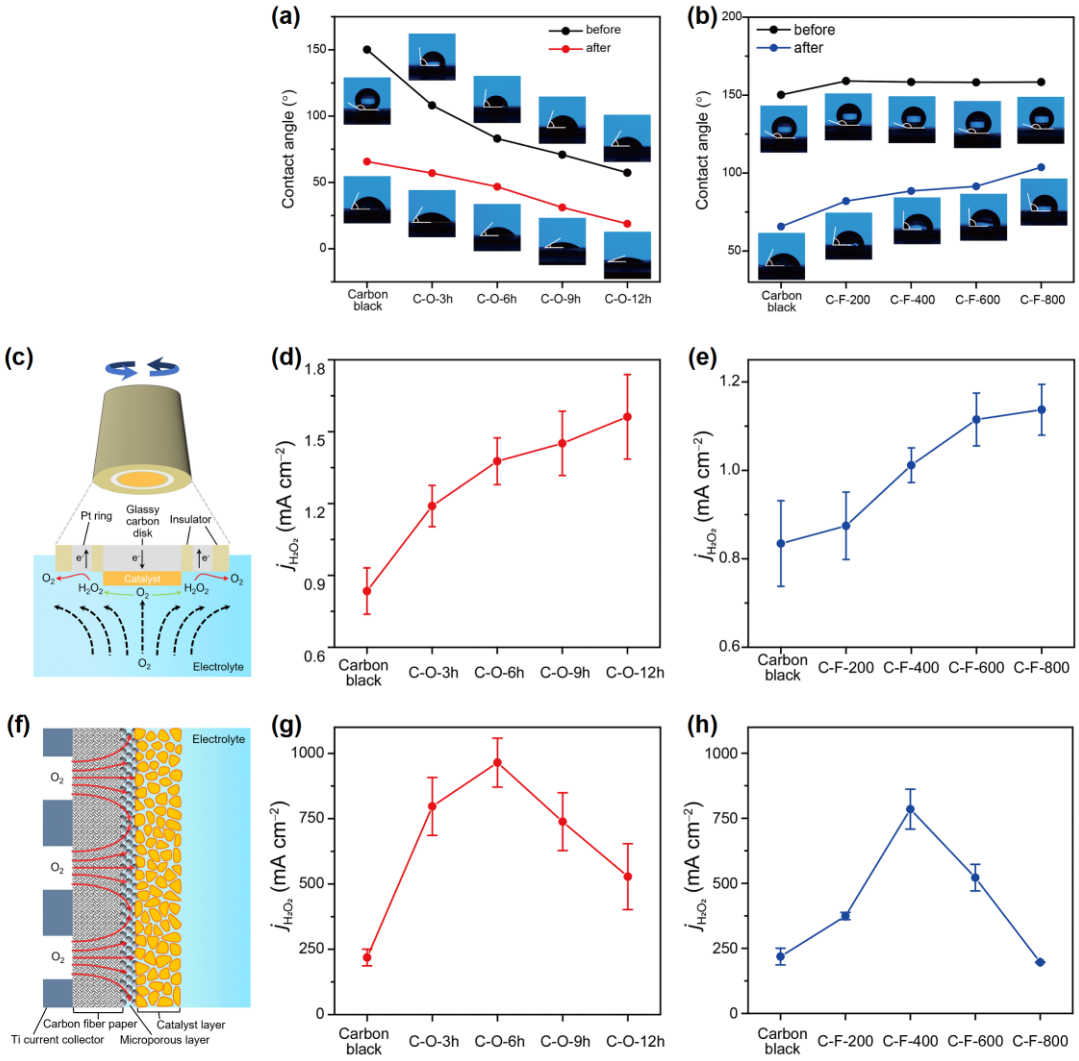

Figure 3. Effect of active sites and microenvironment for H_2O_2 electrosynthesis on doped carbon. (a–b) Contact angles measured on (a) O-doped and (b) F-doped carbon electrodes before and after electrochemical tests. (c) Schematic illustration of the RRDE configuration. (d–e) Partial current densities for H_2O_2 production measured by RRDE on the (d) O-doped and (e) F-doped carbon electrodes. (f) Schematic illustration of the GDE configuration. (g–h) Partial current densities for H_2O_2 production measured in the GDE cell on the (g) O-doped and (h) F-doped carbon electrodes. Adapted with permission from Ref 45. Copyright 2023 American Chemical Society.

In addition to the creation of new active sites, the O/F-doping changed the wetting properties of the microenvironment around catalytic sites, especially for the electrolysis in GDE flow cell, where the mass transport plays a critical role in determining the reaction kinetics. To investigate the impact of the microenvironment, both O- and F-doped carbon catalysts were further tested for H_2O_2 electrosynthesis in the GDE flow cell (Figure 3f). As shown in Figure 3g and 3h, the partial

current density for H_2O_2 production at 0.6 V vs RHE exhibited a volcano-shaped relationship with the O- and F-doping level, respectively. Along with the increase of the O- or F-doping level, the H_2O_2 partial current densities both first increased and then declined at higher doping level, which exhibited a distinct trend from the RRDE-measured activities. This should result from both active sites and O_2 mass transport in the GDE cell that strongly depends on the wetting properties of the catalyst microenvironment. The activity improvement at low doping level is mainly attributed to the more active sites introduced by the O/F-doping, while the decreased activities at high doping level should arise from different factors. The hydrophilic O-doping increased the ECSA with more electrolyte filled in the catalyst layer, which blocked the pores for gas-phase diffusion, resulting in a slower mass transport of O_2. The further increased hydrophobicity on the high-level F-doped electrodes caused insufficient electrolyte in the catalyst layer and thus limited the availability of protons and ionic conductivity, similar to the case of excessive PTFE loading for CO_2RR (Figure 2c). Overall, the active sites and microenvironment interplay to determine the H_2O_2 production rate on the doped-carbon catalysts in the GDE cell. Only a moderately hydrophilic or hydrophobic microenvironment can enable an optimal balance between gaseous reactant and liquid electrolyte in the catalyst layer for efficient H_2O_2 electrosynthesis.[45]

4. Effect of microenvironment on gas-evolving electrocatalysis

The above discussions focused on electrocatalytic reactions with a gaseous reactant, where a moderately hydrophobic microenvironment (indicated by post-reaction contact angle) is favorable because it can facilitate a balance between gaseous reactant and liquid electrolyte in the catalyst layer and thus enhance the electrocatalytic performance. In gas-evolving reactions, gaseous species are continuously generated to form gas bubbles, which will coat the catalyst surface and block the catalytic sites until they are released.[49–51] It thus remains a challenge to improve gas-evolving electrocatalysis with an optimized gas bubble release. Not surprisingly, the wetting characteristic of microenvironment plays a critical role in controlling the gas bubble dynamics and recovery of catalytic sites. For example, superaerophobic or superhydrophilic electrodes with nanostructured morphology (such as nanowires or nanotube arrays) were designed to decrease the adhesion force of gas bubbles and release the generated gas bubbles in a timely manner and at smaller sizes,[29] thus to accelerate the recovery of catalytic sites.

In our recent work, we used the electro-oxidation of N_2H_4 to N_2 gas on carbon-supported Pt nanocatalyst as a model system to investigate the effect of microenvironment on the gas-evolving reaction.[52] In contrast to previous studies,[29] we relied on the widely used electrode formulation with carbon-supported nanocatalyst, and tuned the microenvironment over a wide range of wetting conditions by doping of the carbon support (Vulcan XC-72 carbon black). Again, O-doping makes

the carbon support more hydrophilic while F-doping makes it more hydrophobic. By mixing the Pt/C nanoparticle catalyst and the carbon blacks with different doping levels, we prepared a series of electrodes with the same Pt nanocatalyst but distinct microenvironments over a wide range of hydrophilicity and hydrophobicity. The post-reaction contact angles were measured to be 19.7°, 74.0°, and 143.6° for the Pt/C-O-12, Pt/C, and Pt/C-F-800 electrodes,[52] which reflect their actual wetting states during electrochemical tests. The electrocatalytic performance for N_2H_4 oxidation reaction was evaluated on these electrodes at 0.5 V vs RHE in H-cell. As shown in Figure 4a, the current densities for N_2H_4 oxidation on the electrodes with O- or F-doped carbon were higher than that on the electrode with pristine carbon black. The current density showed a positive correlation with the O- or F-doping level, indicating that both doped-carbon supports in the microenvironment enhanced the electrocatalytic performance of the Pt catalyst for N_2H_4 oxidation.

As the electrodes all have the same Pt catalyst and similar morphology, the difference of the catalytic performance should be attributed to the different wetting properties of the doped-carbon supports. The wetting properties determine how much of the catalyst surface area is wetted by the electrolyte and thus available for aqueous N_2H_4 reactant to adsorb and react. The electrodes with O-doped carbon are more hydrophilic and should have more Pt surface area in contact with the electrolyte, while the hydrophobic F-doped electrodes favor gas and should be less wetted. Indeed, this was validated by the ECSA of Pt measured using Cu underpotential deposition (UPD) method. As shown in Figure 4b, the ECSA of Pt in the Pt/C-O-12 electrode was higher than that in the Pt/C and Pt/C-F-800 electrodes, confirming the effect of microenvironment on the exposure of Pt catalytic sites to the electrolyte. Therefore, the enhanced performance on the O-doped electrodes should be mainly attributed to the more hydrophilic microenvironment that allows more Pt active sites to contact the electrolyte and catalyze N_2H_4 oxidation. Nevertheless, the Pt/C-F-800 electrode showed a lower ECSA than the Pt/C electrode, but still a higher reaction rate for N_2H_4 oxidation. This counterintuitive result implies that the catalytic performance should also be affected by other factors, particularly the bubble dynamics of generated gas.

The N_2 gas bubbles are continuously formed on the catalyst surface during the reaction, which inevitably block some Pt active sites and make them temporarily unavailable to aqueous reactant. Only when the gas bubbles grow so large that the buoyant force is larger than the adhesion force, they will detach from the surface and the blocked Pt sites can be recovered. As a result, the gas bubble formation and detachment process will repeatedly change the contact area of the Pt catalyst with the electrolyte, leading to periodic fluctuations of the reaction rate.[53,54] Indeed, we observed nearly periodic fluctuations of the overpotential in the chronopotentiometric curves measured on the electrodes, as exhibited in Figure 4c, which should reflect the gas bubble dynamics. According to the average fluctuation periods (Figure 4d), the Pt/C-F-800 electrode showed the shortest cycle or lifetime of the gas bubble dynamics, indicating that it took a shorter time for the bubbles to grow

and reach the critical size due to a higher bubble growth rate. Our optical microscopy observations revealed that the hydrophobic microenvironment in the Pt/C-F-800 electrode resulted in a faster diffusion and coalescence of gas bubbles,[52] and thus accelerated the detachment of the generated gas bubbles and the recovery of Pt active sites. The faster gas bubble release could compensate the negative impact of the lower ECSA, so that the Pt/C-F-800 electrode still showed a higher current density than the Pt/C electrode (Figure 4a). This example further indicates that the mass transport of both liquid and gaseous species is sensitive to the wetting properties of the microenvironment in gas-evolving reactions.

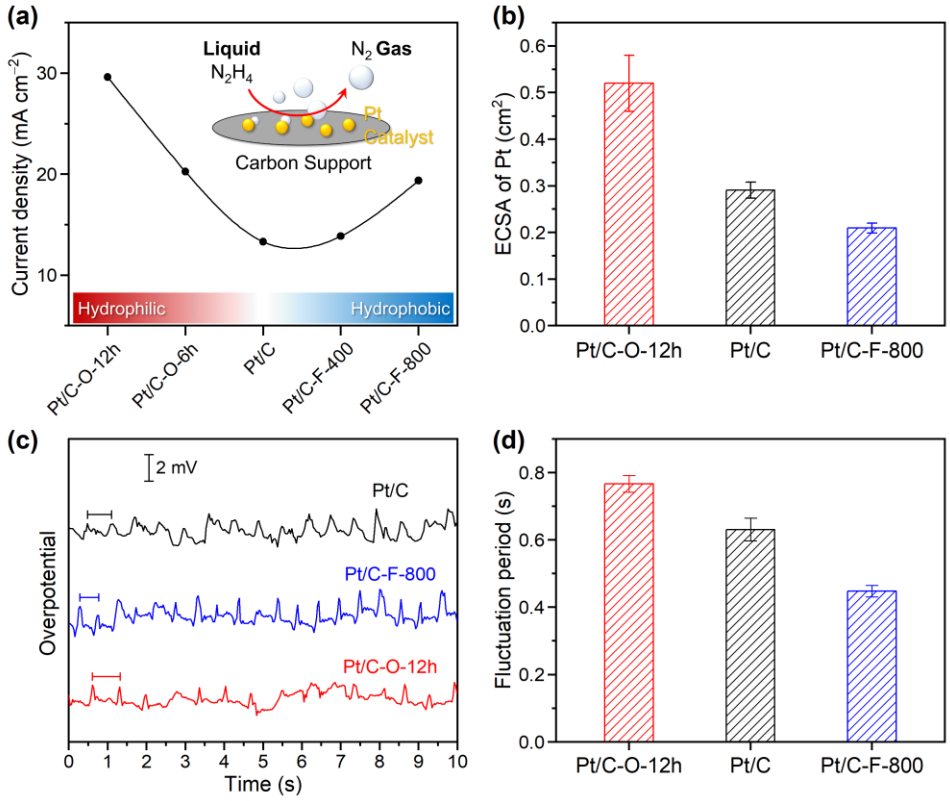

Figure 4. Effect of microenvironment on N_2H_4 electro-oxidation reaction. (a) Comparison of bulk electrolysis current densities measured at 0.5 V vs RHE on the electrodes with the same Pt catalyst but different O- or F-doping levels of carbon support. (b) The ECSA of Pt catalyst in the electrodes determined using the Cu UPD method. (c) Chronopotentiometric curves recorded on the electrodes for N_2H_4 electro-oxidation at a current density of 10 mA cm^{-2} in a H-cell. (d) Average fluctuation periods of the overpotential presented in (c). Adapted with permission from Ref 52. Copyright 2023 American Chemical Society.

5. Summary and Outlook

In the above, we discussed the effect of catalyst microenvironment, particularly the wetting properties around the catalytic sites, on the mass transport and kinetics of gas-involving reactions. Different methods were developed to control the microenvironment over a wide range of wetting characteristics, such as dispersing PTFE nanoparticles and using doped-carbon support, which are generally applicable to improve other electrocatalytic reactions. The hydrophilic and hydrophobic microenvironments may dominate different factors in the electrocatalytic process ─ the exposure of active sites to the electrolyte and the mass transport of gaseous specious, respectively. Therefore, both factors should be taken into consideration for the investigation of gas-involving reactions and the development of efficient electrolyzers. These understandings and insights can be used to guide a rational design and fine tuning of the hydrophilic and hydrophobic microenvironments and utilize their advantages to improve other strategically important electrochemical systems with gas-phase reactants or products. For example, we suggest that a hydrophobic microenvironment can be used to improve the mass transport and kinetics of the NRR with N_2 gas reactant,[39] while an optimized microenvironment can enhance the formate oxidation reaction with CO_2 gas product. Furthermore, hydrophilic/hydrophobic cooperative electrode could be developed using interface engineering to achieve highly efficient HER electrolysis.[29] The combination of both hydrophilic and hydrophobic properties can be further used to design a bubble-less electrode for efficient membrane-less water electrolysis.[55]

In summary, we highlighted some mechanistic insights into the catalyst microenvironment for gas-involving electrocatalysis in this Concept article. We discussed the generally applicable effect of the wetting properties for various reactions, where the mass transport of both gaseous and liquid species plays a critical role in determining the electrocatalytic performance. A moderately hydrophobic microenvironment (indicated by post-reaction contact angle) can accelerate the mass transport of gaseous reactant to the active sites and facilitate the removal of generated gas bubbles to recover the active sites. However, a too hydrophobic microenvironment decreases the contact of active sites with liquid electrolyte and limits the availability of protons and ionic conductivity, negatively impacting the catalytic performance. In contrast, a hydrophilic microenvironment is favorable for the exposure of active sites to liquid electrolyte and can promote gas-evolving reactions with liquid reactant. The local gas/liquid balance around catalytic sites can be further optimized by finely tuning the wetting properties of the microenvironment. These insights provide inspirations and guidance for the rational design of efficient electrocatalysts and electrolyzers for renewable energy conversion.

Acknowledgements

The authors acknowledge the support of the National Science Foundation (NSF) under Grant No. 1943732.

Conflict of Interest

The authors declare no conflict of interest.

Keywords: Electrocatalysis • Gas-Involving Reaction • Microenvironment • Hydrophobicity • Mass Transport

References

1. X. X. Wang, M. T. Swihart, G. Wu, *Nat. Catal.* **2019**, *2*, 578−589.
2. A. P. O'Mullane, M. Escudero-Escribano, I. E. L. Stephens, K. Krischer, *ChemPhysChem* **2019**, *20*, 2900−2903.
3. J. H. Montoya, A. A. Peterson, J. K. Nørskov, *ChemCatChem* **2013**, *5*, 737−742.
4. Q. Lu, J. Rosen, F. Jiao, *ChemCatChem* **2015**, *7*, 38−47.
5. H. Shin, K. U. Hansen, F. Jiao, *Nat. Sustain.* **2021**, *4*, 911−919.
6. L. Hu, Z. Xing, X. Feng, *ACS Energy Lett.* **2020**, *5*, 430−436.
7. S. Li, Y. Wang, Y. Du, X. D. Zhu, J. Gao, Y. C. Zhang, G. Wu, *Small* **2023**, *19*, 2206776.
8. L. Hu, H. S. Pillai, C. Feit, K. Shi, Z. Gao, P. Banerjee, H. Xin, X. Feng, *ACS Energy Lett.* **2022**, *7*, 4290−4298.
9. Z. Lu, G. Chen, S. Siahrostami, Z. Chen, K. Liu, J. Xie, L. Liao, T. Wu, D. Lin, Y. Liu, T. F. Jaramillo, J. K. Nørskov, Y. Cui, *Nat. Catal.* **2018**, *1*, 156−162.
10. S. Siahrostami, S. J. Villegas, A. H. B. Mostaghimi, S. Back, A. B. Farimani, H. Wang, K. A. Persson, J. Montoya, *ACS Catal.* **2020**, *10*, 7495−7511.
11. Y. Xia, X. Zhao, C. Xia, Z. Y. Wu, P. Zhu, J. Y. Kim, X. Bai, G. Gao, Y. Hu, J. Zhong, Y. Liu, H. Wang, *Nat. Commun.* **2021**, *12*, 4225.
12. X. Zhao, Y. Liu, *J. Am. Chem. Soc.* **2021**, *143*, 9423−9428.
13. C. Zhang, X. Shen, Y. Pan, Z. Peng, *Front. Energy* **2017**, *11*, 268−285.
14. M. B. Ross, P. De Luna, Y. Li, C. T. Dinh, D. Kim, P. Yang, E. H. *Nat. Catal.* **2019**, *2*, 648−658.

15. S. Garg, M. Li, A. Z. Weber, L. Ge, L. Li, V. Rudolph, G. Wang, T. E. Rufford, *J. Mater. Chem. A* **2020**, *8*, 1511−1544.
16. J. Resasco, L. D. Chen, E. Clark, C. Tsai, C. Hahn, T. F. Jaramillo, K. Chan, A. T. Bell, *J. Am. Chem. Soc.* **2017**, *139*, 11277−11287.
17. C. Kim, J. C. Bui, X. Luo, J. K. Cooper, A. Kusoglu, A. Z. Weber, A. T. Bell, *Nat. Energy* **2021**, *6*, 1026−1034.
18. X. Chen, J. Chen, N. M. Alghoraibi, D. A. Henckel, R. Zhang, U. O. Nwabara, K. E. Madsen, P. J. A. Kenis, S. C. Zimmerman, A. A. Gewirth, *Nat. Catal.* **2021**, *4*, 20−27.
19. N. Govindarajan, A. Xu, K. Chan, *Science* **2022**, *375*, 379−380.
20. Z. Xing, L. Hu, D. S. Ripatti, X. Hu, X. Feng, *Nat. Commun.* **2021**, *12*, 136.
21. R. Iwata, L. Zhang, K. L. Wilke, S. Gong, M. He, B. M. Gallant, E. N. Wang, *Joule* **2021**, *5*, 887−900.
22. K. Y. Law, *J. Phys. Chem. Lett.* **2014**, *5*, 686−688.
23. Z. Xing, X. Hu, X. Feng, *ACS Energy Lett.* **2021**, *6*, 1694−1702.
24. K. Yang, R. Kas, W. A. Smith, and T. Burdyny, *ACS Energy Lett.* **2021**, *6*, 33−40.
25. G. Liu, W. S. Y. Wong, M. Kraft, J. W. Ager, D. Vollmer, R. Xu, *Chem. Soc. Rev.* **2021**, *50*, 10674−10699.
26. Z. Xing, K. Shi, X. Hu, X. Feng, *J. Energy Chem.* **2022**, *66*, 45−51.
27. P. Wang, T. Hayashi, Q. Meng, Q. Wang, H. Liu, K. Hashimoto, L. Jiang, *Small* **2017**, *13*, 1601250.
28. T. Burdyny, P. J. Graham, Y. Pang, C. Dinh, M. Liu, E. H. Sargent, and D. Sinton, *ACS Sustainable Chem. Eng.* **2017**, *5*, 4031−4040
29. C. Zhang, Z. Xu, N. Han, Y. Tian, T. Kallio, C. Yu, L. Jiang, *Sci. Adv.* **2023**, *9*, eadd6978.
30. B. A. Zhang, T. Ozel, J. S. Elias, C. Costentin, D. G. Nocera, *ACS Cent. Sci.* **2019**, *5*, 1097–1105.
31. B. Kim, F. Hillman, M. Ariyoshi, S. Fujikawa, P. J. A. Kenis, *J. Power Sources* **2016**, *312*, 192−198.
32. K. U. Hansen, F. Jiao, *Joule* **2021**, *5*, 754−757.
33. X. Liu, P. Schlexer, J. Xiao, Y. Ji, L. Wang, R. B. Sandberg, M. Tang, K. S. Brown, H. Peng, S. Ringe, C. Hahn, T. F. Jaramillo, J. K. Nørskov, K. Chan, *Nat. Commun.* **2019**, *10*, 32.

34. B. Kim, F. Hillman, M. Ariyoshi, S. Fujikawa, P. J. A. Kenis, *J. Power Sources* **2016**, *312*, 192−198.
35. Y. Wu, L. Charlesworth, I. Maglaya, M. N. Idros, M. Li, T. Burdyny, G. Wang, T. E. Rufford, *ACS Energy Lett.* **2022**, *7*, 2884−2892.
36. S. C. Perry, S. Mavrikis, M. Wegener, P. Nazarovs, L. Wang, C. P. de León, *Faraday Discuss.* **2021**, *230*, 375−387.
37. J. Pellessier, X. Gong, B. Li, J. Zhang, Y. Gang, K. Hambleton, C. Podder, Z. Gao, H. Zhou, G. Wang, H. Pan, Y. Li, *J. Mater. Chem. A* **2023**, *11*, 26252−26264.
38. F. Huq, I. Sanjuán, S. Baha, M. Braun, A. Kostka, V. Chanda, J. R. C. Junqueira, N. Sikdar, A. Ludwig, C. Andronescu, *ChemElectroChem* **2022**, *9*, e202101279.
39. H. Wu, A. Singh-Morgan, K. Qi, Z. Zeng, V. Mougel, D. Voiry, *ACS Catal.* **2023**, *13*, 5375−5396.
40. S. C. Perry, D. Pangotra, L. Vieira, L. I. Csepei, V. Sieber, L. Wang, C. P. de León, F. C. Walsh, *Nat. Rev. Chem.* **2019**, *3*, 442−458.
41. H. W. Kim, M. B. Ross, N. Kornienko, L. Zhang, J. Guo, P. Yang, B. D. McCloskey, *Nat. Catal.* **2018**, *1*, 282−290.
42. S. Yang, A. Verdaguer-Casadevall, L. Arnarson, L. Silvioli, V. Čolić, R. Frydendal, J. Rossmeisl, I. Chorkendorff, I. E. L. Stephens, *ACS Catal.* **2018**, *8*, 4064−4081.
43. C. Xia, Y. Xia, P. Zhu, L. Fan, H. Wang, *Science* **2019**, *366*, 226−231.
44. J. Duan, S. Chen, M. Jaroniec, S. Z. Qiao, *ACS Catal.* **2015**, *5*, 5207−5234.
45. Z. Xing, K. Shi, Z. S. Parsons, X. Feng, *ACS Catal.* **2023**, *13*, 2780−2789.
46. K. Zhao, Y. Su, X. Quan, Y. Liu, S. Chen, H. Yu, *J. Catal.* **2018**, *357*, 118−126.
47. E. Jung, H. Shin, W. H. Antink, Y. E. Sung, T. Hyeon, *ACS Energy Lett.* **2020**, *5*, 1881−1892.
48. W. Wang, X. Lu, P. Su, Y. Li, J. Cai, Q. Zhang, M Zhou, O. Arotiba, *Chemosphere* **2020**, *259*, 127423.
49. D. Fernandez, P. Maurer, M. Martine, J. M. D. Coey, M. E. Möbius, *Langmuir* **2014**, *30*, 13065−13074.
50. X. Zhao, H. Ren, L. Luo, *Langmuir* **2019**, *35*, 5392−5408.
51. Q. Chen, L. Luo, *Langmuir* **2018**, *34*, 4554−4559.
52. K. Shi, Z. S. Parsons, X. Feng, *ACS Energy Lett.* **2023**, *8*, 2919−2926.

53. C. Gabrielli, F. Huet, R. P. Nogueira, *Electrochim. Acta* **2005**, *50*, 3726−3736.
54. J. T. H. Kwan, A. Nouri-Khorasani, A. Bonakdarpour, D. G. McClement, G. Afonso, D. P. Wilkinson, *J. Electrochem. Soc.* **2022**, *169*, 054531.
55. K. Deng, H. Feng, Y. Zhang, D. Liu, Q. Li, *Joule* **2023**, *7*, 1852−1866.

Table of Contents Graphic:

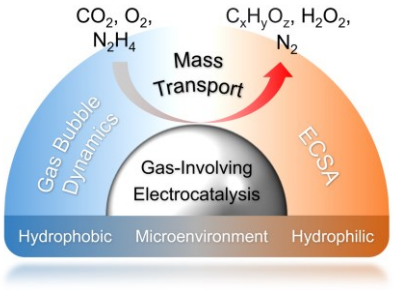

In gas-involving electrocatalysis, the catalyst microenvironment plays a critical role in determining the mass transport and reaction kinetics, which however has been largely overlooked. This Concept sheds insights into the effect and optimization of microenvironment for electrocatalytic reactions, including CO_2 reduction, 2-electron oxygen reduction, and hydrazine oxidation.